Time-resolved measurement of acoustic pulses generated by MeV protons stopping in aluminum

G. E. Sieger* and H. W. Lefevre
Department of Physics, University of Oregon, Eugene, Oregon 97403
(Received 17 October 1984)

A wide-band capacitive detector has been constructed to make time-resolved measurements of acoustic pulses generated in aluminum and in other solids by ns pulses of MeV protons. The near-field signal observed traveling in the beam direction is a measure of the initial pressure distribution along the path of the stopping protons. The measured amplitudes and shapes of such signals are consistent with the thermoelastic model of sound generation. From the signal rise time (<2 ns), it can be concluded that the conversion into heat of the energy loss of a slowing proton is localized within a radius of several micrometers. For the data presented, the fraction of beam-pulse energy absorbed from acoustic radiation by the detector is about 5×10^{-14}. Acoustic signals which generate 10^{-2} eV of electrical energy in the detector (~4 μV into 50 Ω for 5 ns) are easily discernible after signal averaging. Acoustic signals were used to probe the formation of microbubbles in hydrogen-implanted aluminum. From bubble growths inferred from acoustic measurements, the diffusivity of hydrogen in aluminum is estimated at a temperature where the diffusivity is 8 orders of magnitude smaller than in previous measurements.

I. INTRODUCTION

There has been much interest recently in the possible mechanisms of sound generation due to energetic charged particles slowing down in matter. The most extensive experiments have investigated the interaction of proton beams with fluids. Sulak *et al.*[1] have reported on a study of acoustic radiation in various liquids produced by slowing of a 28-GeV proton beam, and by the stopping of 200- and 158-MeV protons. Golubnichii *et al.*[2] have investigated sound generated in liquids by a 50-MeV electron beam. In those studies the observed signal characteristics indicated that the acoustic waves were generated thermoelastically, i.e., by adiabatic expansion following rapid localized heating. In asking whether these effects could be seen in solid targets and at lower ion energies, where energy deposition per unit path length is larger, we have looked for and found that acoustic radiation.

Targets of various solid materials were bombarded with pulsed proton beams of up to 5 MeV from the University of Oregon Van de Graaff accelerator. The ratio of proton range to speed of sound for 4-MeV protons in aluminum is about 20 ns, and our beam-pulse duration is 1 ns. Thus, by observing acoustic pulses traveling in the beam direction, one can resolve wavefronts originating from different depths in the target. A capacitive detector and a wide-band ($\sim10^9$ Hz) preamplifier were constructed in order to make time-resolved measurements of such signals. Acoustic measurements were made on targets of aluminum, beryllium, copper, tantalum, silicon, and fused silica. Only data from aluminum, in which the thermoelastic response is several times larger than in the other materials, are presented in this paper.

Relatively little has been reported on sound generation in solids by penetrating charged particles. Beron *et al.*[3] have observed standing waves in an aluminum cylinder excited by 1-μs pulses of 100—1000-MeV electrons. Volovik and Lazurik-Él'tsufin[4] measured the maximum displacement of a thin metal plate used to slow millisecond pulses of 30—250-MeV protons and electrons. In those cases the displacement amplitudes were found to be proportional to energy deposition, in agreement with the thermoelastic model of sound generation. In experiments reported by Perry,[5] thick targets of aluminum and copper were irradiated with very intense electron-beam pulses of 40-ns duration and 1.5-MeV average energy, and the shapes of the resulting acoustic pulses were measured. By assuming a thermoelastic mechanism, he was able to estimate the depth profile of deposited energy, which was in agreement with calorimetric measurements.

In a recent report de Rujula *et al.*[6] examine in detail the possibility of using neutrino beams for whole-earth tomography. They propose measuring the acoustic radiation generated by the charged particle showers which would result from the interaction of high-energy neutrinos with the earth. They remark, however, that "our present knowledge of sound generation by particle beams in solids is negligible, compared with the situation for liquids."

The design of our detector was suggested by the work of Gauster and Breazeale[7] and Cantrell and Breazeale.[8] They developed a capacitive transducer which could be used both to excite and to detect acoustic waves in metal samples. Using narrow-band amplifiers, they measured sound speeds and harmonic distortion at frequencies up to 10^8 Hz. Conventional piezoelectric transducers are usually limited to bandwidths $\simeq10^6$ Hz, although Tam and Coufal[9] have recently used a thin-film piezoelectric transducer with 10^8-Hz bandwidth, in order to detect laser-excited 10-ns acoustic pulses in a metal plate.

II. EXPERIMENTAL

Acoustic pulses are detected by the modulation they produce in the spacing between the plates of a charged

capacitor.[10,11] Figure 1 shows the detector mounted on the end of an accelerator beam tube. A 2.5-cm-diam target, sealed by a Viton O-ring, forms part of the vacuum containment. A brass post 2.6 mm in diameter is spaced 10 μm away from the back side of the target by compression against a Teflon dielectric, and is biased at 1000 V or less. This detector post is the central conductor in a 50-Ω coaxial transmission line, whose grounded outer conductor is pressed into contact with the target. Bias voltage is applied through a 2-MΩ resistor in a T connector, as shown in Fig. 2, and is isolated from the preamplifier by a 0.0052-μF coupling capacitor.

The Thevenin equivalent-circuit voltage of the detector is

$$V_{\rm eqv}(t)=V_B L_1(t)/L_0 \ . \tag{1}$$

Here V_B is the bias voltage, and $L(t)=L_0+L_1(t)$ is the spacing between the target and the detector post, where it is assumed that $L_1 \ll L_0$. The equivalent-circuit voltage is divided across the detector capacitance, C, and the 50-Ω line impedance, R. It can be shown that the target surface velocity inferred from a detector output voltage $V(t)$ is

$$\frac{dL}{dt}=\frac{L_0}{V_B}\left[\frac{1}{RC}+\frac{d}{dt}\right]V(t) \ . \tag{2}$$

It should be noted that the time constant of our detector is so short ($RC \cong 0.25$ ns) that the output voltage is nearly proportional to the target surface velocity. The first term in the above expression dominates.

Signals from the detector are amplified by two Motorola DC-400 MHz wideband amplifiers (MWA 110) in cascade, as shown in Fig. 2. The overall gain is 28 dB with nominal input and output impedances of 50 Ω. Care was taken to optimize the high-frequency response of the circuit. For example, the width of the conducting strips in the signal path, and their distance from a parallel ground plane were chosen for correct impedance matching. As a result, a preamp rise time of 0.7 ns was obtained.

The major source of asynchronous noise in the signal is broadband thermal noise (Johnson noise). The rms voltage fluctuation across a resistance R is given approximately by[12]

$$V_{\rm rms}=(4RkT\,\Delta f)^{1/2} \ , \tag{3}$$

where T is the temperature, k is Boltzmann's constant, and Δf is the circuit bandwidth. At room temperature and for a bandwidth of 10^9 Hz, Eq. (3) gives $V_{\rm rms}=30\ \mu$V. In order to observe signals well below the level of thermal noise, a system for averaging the acoustically generated signals from many beam pulses was used.

A simplified block diagram of the electronics used for signal sampling and digitizing is shown in Fig. 3. The preamp output is sampled by a Tektronix Type 661 oscilloscope with a type 4S1 sampling unit, which has a rise time of 0.3 ns. The triggering signal for the scope is derived from the passage of the pulsed beam through a ferrite-core transformer. The time interval between triggering and sampling is controlled by a computer-generated voltage applied to the external horizontal sweep of the scope. The most recently sampled voltage, after being offset and amplified, is monitored at the sampler output. This voltage is allowed to pass through a linear gate when two logic signals are present in coincidence. One logic pulse indicates that sufficient time has elapsed after triggering for the sampler output to have stabilized. The second logic signal indicates that the analog-to-digital

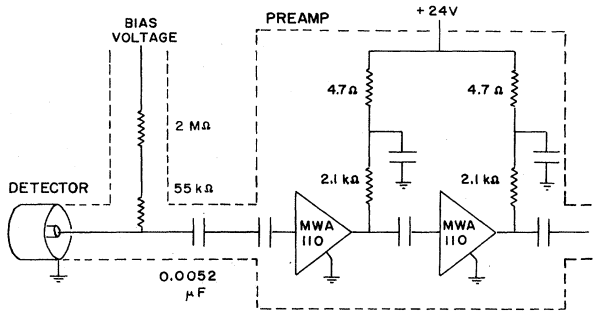

FIG. 2. Schematic drawing of detector and preamplifier circuit. All capacitors in the preamp are 0.1 μF ceramic chip capacitors.

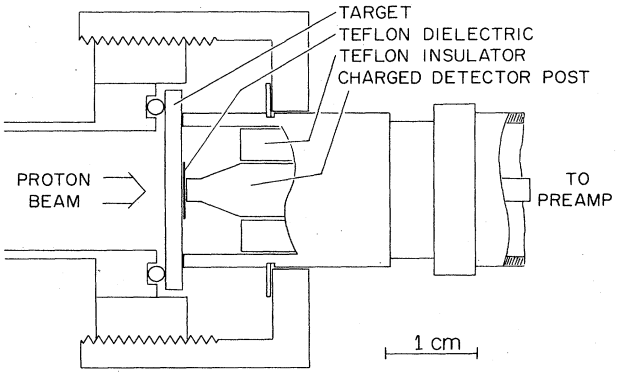

FIG. 1. Schematic drawing of the capacitive detector, shown mounted on the end of the beam line.

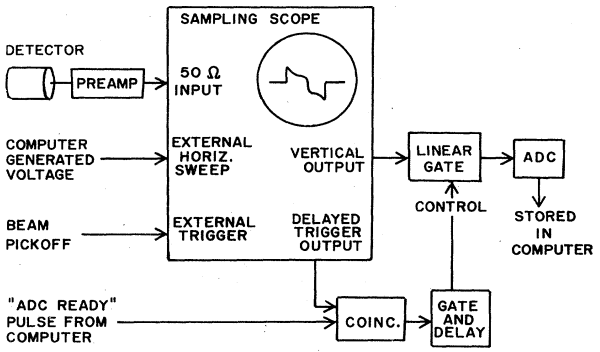

FIG. 3. Simplified block diagram of the electronics used to sample, digitize, and record acoustic signals.

converter (ADC) is ready to receive an input. Gated voltage signals are digitized by a 10-bit ADC and stored in the computer.

This system requires about 120 μs to digitize and store a sampled voltage. For a typical measurement about 20 000 digitized voltages are averaged at each of 512 acoustic times of flight, which requires about 20 minutes. By these means asynchronous noise is reduced by more than a hundredfold. Synchronous noise is eliminated by recording data with both polarities of detector voltage and subtracting one result from the other.

Some of the problems we encountered in developing this new type of acoustic measurement are worth mentioning. One difficulty was that of finding a suitable dielectric material. A dielectric of mica or Mylar was found to acquire a net charge in response to an applied voltage, which would cancel the electric field at the target surface. Similar behavior was observed for a Teflon dielectric contaminated with moisture. In experiments in which a target was heated above about 80 °C, a Teflon dielectric would acquire a permanent (negative) charge, which remained after cooling to room temperature. Also, we found it necessary to replace a Teflon dielectric after a day of use. Beyond that time the Teflon would often break down under voltage. As a result of such dielectric breakdowns, both MWA 110 stages of the preamp would fail open, which fortunately prevented damage to the sampling scope.

For our acoustic measurements it is important that the faces of a target be flat and parallel. The following procedure for making aluminum targets gave good results. Squares of aluminum sawed from a flat sheet were machined on a lathe into discs and were then polished on a wheel. The polishing agent was a combination of mineral oil and silicon carbide of successively finer grits. Another requirement is that targets have surfaces of good electrical conductivity. This was accomplished by evaporating aluminum in a thin layer onto targets of silicon and fused silica.

One difficulty in experimental procedure was the alignment of the proton beam with the target and detector. The beam was initially focused onto a quartz scintillator at the target position. The end section of the beam line was then aligned by adjusting three turnbuckles which supported a bellows in the beam line. It is also worth noting that we observed a puzzling loss of signal as targets were heated in place. That problem was solved by occasionally tightening the threaded detector cap to compensate for thermal expansion.

III. THEORY

Suppose that internal stresses are generated in an elastic medium by localized heating. Assuming the medium to be isotropic and homogenous, the force per unit volume can be written[13]

$$\rho\frac{\partial^2\sigma}{\partial t^2}=\left[B+\tfrac{4}{3}\mu\right]\nabla\left[\nabla\cdot\sigma-\frac{\gamma}{C\rho}q(\mathbf{r},t)\right]-\mu\nabla\times(\nabla\times\sigma)\ , \tag{4}$$

where $\sigma(\mathbf{r},t)$ is the displacement, $q(\mathbf{r},t)$ is the excess heat per unit volume, ρ is the density, C is the specific-heat capacity, and B and μ are the bulk and shear moduli. The thermoelastic constant γ is given by

$$\gamma=\alpha\frac{1+\nu}{1-\nu}\ ,$$

where α is the linear thermal expansion coefficient and ν is Poisson's ratio.

Assuming $\nabla\times\sigma\equiv 0$ initially, no shear waves will be generated by local heating. In that case stresses in the medium can be completely described by specifying the pressure at each point:

$$p(\mathbf{r},t)=-E\left[\nabla\cdot\sigma-\frac{\gamma}{C\rho}q(\mathbf{r},t)\right]\ , \tag{5}$$

where $E=B+4\mu/3$ is the plate modulus. Substituting Eq. (5) in Eq. (4) yields the following wave equation:

$$\nabla^2 p-\frac{1}{V_l^2}\frac{\partial^2 p}{\partial t^2}=-\frac{\gamma}{C}\frac{\partial^2 q}{\partial t^2}\ , \tag{6}$$

where $V_l=(E/\rho)^{1/2}$ is the longitudinal sound speed. The nonhomogeneous solution of Eq. (6) can be written as a volume integral over the source:[1,14]

$$p(\mathbf{r},t)=\frac{\gamma}{4\pi C}\int\frac{d\mathbf{r}'}{R}\frac{\partial^2}{\partial t^2}q(\mathbf{r}',t-R/V_l)\ , \tag{7}$$

where $R=|\mathbf{r}-\mathbf{r}'|$.

As an energetic proton slows down in a material, it gives up its energy to electronic excitations. The time required for an MeV proton to stop in a solid is so short ($\sim 10^{-11}$ s) that the energy deposition can be considered to be instantaneous. There is some controversy, however, concerning the rate at which the energy of the electron is converted into phonons, thus becoming heat. Measurements by Liu *et al.*[15] of changes in the reflectivity of and charged particle emission from a silicon crystal indicate that the energy conversion time is $<10^{-11}$ s. Thus for our purposes, the rate of local heating in a target due to a stopping proton pulse of very short duration can be written

$$\dot{q}(\mathbf{r},t)=N(y,z)\frac{dE}{dx}(E_0,x)\delta(t)\ . \tag{8}$$

Here dE/dx is the proton stopping power as a function of the incident energy E_0 and the depth x in the target, $N(y,z)$ is the beam-pulse density in protons/cm^2, and δ is the Dirac function. Substituting Eq. (8) into Eq. (7), one finds that a stopping beam pulse produces an initial pressure distribution which is proportional at each point to the local heating:

$$p(\mathbf{r},0)=N\frac{\gamma}{C}V_l^2\frac{dE}{dx}\ . \tag{9}$$

For $t>0$, $p(\mathbf{r},t)$ is the solution of the homogeneous wave equation with initial conditions of Eq. (9) and $\dot{p}(\mathbf{r},0)\equiv 0$.

In the above treatment the thermoelastic response is assumed to be adiabatic. Thermal diffusion becomes important only for acoustic components with frequencies $\gtrsim f_0=V_l^2/2\pi D$, where D is the thermal diffusion coeffi-

cient.[16] Since $f_0 \sim 10^9 - 10^{10}$ Hz for most metals, nonadiabatic processes are not observable in our measurments. When the free surface of a solid is heated periodically at frequencies $\ll f_0$, the forward and backward launched thermoacoustic waves nearly cancel. In that case, the small signal which propagates through the solid is a measure of the heat flow near the free surface. Such signals are used in so-called "thermal wave" imaging to infer the depth profile of thermal diffusivity near a sample surface.[16,17]

IV. RESULTS

Figure 4(a) shows an acoustic signal from a 2.5-mm-thick Al target bombarded with a pulsed beam of 3.74-MeV protons (10^7 protons/pulse, 16-μs pulse spacing).[18] The signal arrives at the detector about 200 ns after beam entry into the target, and it is followed by about a dozen discernable reflections from the parallel target faces, spaced about 400 ns apart. The first such reflection is shown in Fig. 4(c). From the acoustic transit time of the target one can determine the longitudinal sound speed.

Since the beam diameter (3 mm) is much larger than the proton range (~ 100 μm); an initial pressure distribution propagates as two nearly plane-wave pulses which travel in opposite directions. For that case the acoustic response of the material near the detector is nearly a traveling plane wave propagating normal to the target surface.

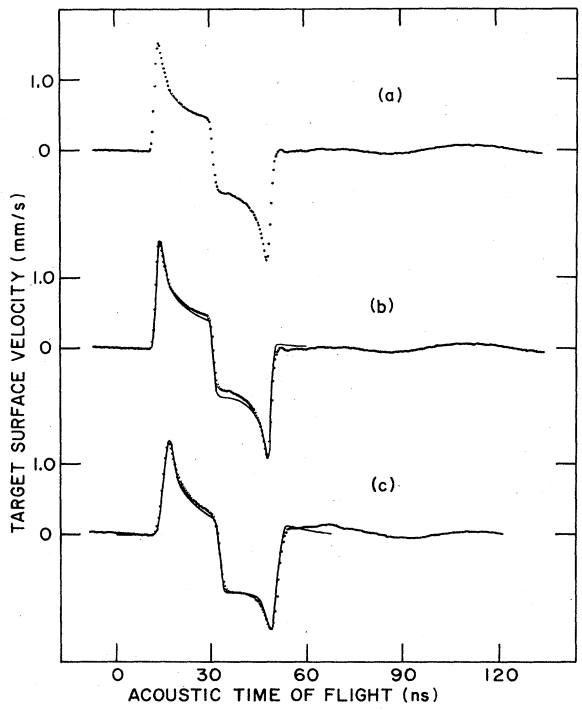

FIG. 4. (a) Acoustic signal generated by a 3.74-MeV proton beam stopping in aluminum. The origin on the abscissa is arbitrary. (b) Same signal as in (a), together with a calculated waveform. (c) Reflected acoustic signal which arrives at the detector about 400 ns after the signal in (a), together with a calculated waveform. The origin on the abscissa is arbitrary.

We measure displacement velocity, which for a traveling wave is proportional at each point to pressure

$$\dot{\xi}(x - V_l t) = p(x - V_l t)/Z_l \,, \tag{10}$$

where $Z_l = \rho V_l$ is the characteristic (longitudinal) impedance. One may interpret the signal shown in Fig. 4(a) in the following way. The first half is due to a forward launched compression wave. The last half is due to the backward launched compression wave which was converted to a rarefaction wave upon reflection from the free front surface of the target. The peak at the shortest (and longest) arrival time is the so-called Bragg peak of the stopping beam. For a single proton stopping in aluminum, dE/dx is sharply peaked about 0.5 μm from the end of proton range. For a beam of protons, the individual Bragg peaks are spread in depth over several micrometers, due to the range straggling.[19] In Fig. 4 it can be seen that signal (a) is not quite symmetric and that the reflected signal (c) is further distorted. These signals are intermediate in shape between the near-field signal described by a slab geometry, and the far-field signal. For an acoustic path length much greater than the beam diameter, the observed signal would be the time derivative of the near-field signal.

It should be noted that acoustic pulses of the sort shown in Fig. 4 cause a target surface displacement of only about 0.1 Å (0.5 mm/s for 20 ns). For signals of such small amplitude the target surface in contact with the Teflon dielectric acts as a nearly free surface.

The signal in Fig. 4(a) is shown again in (b) together with a calculated waveform. A calculated waveform is also shown for the reflected signal in (c). The predicted waveforms were obtained by averaging the response given by Eqs. (6) and (9) over the detector surface. Reflections were accounted for by use of appropriate image sources. The actual beam intensity profile was not measured and is assumed for the calculations to be uniform over the area of the collimating aperture. Also, the magnitude of the calculated waveforms are scaled for best fit. The uncertainty in the absolute measurement is about 10%, due primarily to two factors; (1) the beam current cannot be monitored during acoustic measurements, since the target is grounded by the detector, and (2) the actual detector capacitance is uncertain by several percent because of the nonrigidity of the dielectric material.

The calculated waveform in Fig. 4(b) has also been Gaussian smoothed to account for the combined effects of the beam-pulse duration, range straggling of the stopping protons, and the preamp response. The calculated waveform in 4(c) has been smoothed by successive three point averages to match the observed rise time of the measured signal.

It can be seen that the acoustic signals in Fig. 4 are superimposed on a background of long-wavelength oscillations, which are due to a standing-wave pattern excited in the target by the recurring beam pulses. Both the amplitude and phase of these waves were observed to change as the target was heated. In one target, for which the beam-pulse period was nearly a multiple of the acoustic transit time, the standing waves were much larger in amplitude. Allowing for standing waves, the signals in Fig. 4 are in

good agreement with the predicted waveforms.

When other target materials (Al, Be, Cu, Ta, Si, and fused silica) were bombarded with protons, we observed acoustic signals similar to those from aluminum. The amplitudes of those signals were in agreement with the thermoelastic model within an overall uncertainty of about 20%.

V. HYDROGEN IMPLANTATION

Similar measurements were made on aluminum targets which had been implanted with hydrogen. In those targets the acoustic properties were modified in a narrow region near the end of range of the implanting beam. The implantation dose rate was 2.3×10^{14} protons/cm^2/s, a beam current about 50 times greater than that of the pulsed beam used for acoustic measurements. The back face of the target was water cooled during implantation, and temperatures inside the target were nowhere $>30°$ C. Also, the beam was rastered across the collimating aperture to insure uniform implantation inside an area 3 mm in diameter.

Figure 5(a) shows the signal from an aluminum target which had been implanted with 5×10^{18}/cm^2 of 4.39-MeV protons. This signal was generated by 3.74-MeV protons, whose range is about three quarters of the implantation depth. Thus, the primary signal (labeled A_1) is separated in time from the signal (A_2) that was reflected by the hydrogen implanted layer. A signal (A_3) is also discernable in Fig. 5(a) which has been reflected twice by the implanted layer. Some of the possible acoustic paths are shown schematically in Fig. 6. Figure 5(b) shows the signal arriving at the detector about 400 ns after the signal in (a). The primary component of the signal (B_2), which is detected after reflecting from both target faces, is preceded by a reflection (B_1) from the backside of the implanted layer and is followed by a superposition of two other components (B_3 and B_4). Again, the corresponding acoustic paths are shown in Fig. 6.

The signals in Fig. 5 can be explained qualitatively in the following way. For a plane-wave signal normally incident on a thin layer of different acoustic impedance, in an otherwise homogeneous material, the reflected signal is proportional to the time derivative of the incident signal. The signal transmitted through the layer suffers some attenuation of its high-frequency components. In Fig. 5 it can be seen that the observed reflections from the implanted layer have the appearance of derivatives of the primary signal, the peaks being broadened somewhat due to the finite width of the layer. The polarity of the reflections indicates a layer of reduced acoustic impedance, which we attribute to the formation of hydrogen microbubbles.

The agglomeration of hydrogen in aluminum has been investigated by Ells and Evans.[20] They irradiated aluminum samples with 7-MeV protons to produce hydrogen concentrations of up to 25 ppm (by weight). Etching of electropolished sections left pits $\leq1\,\mu$m in diameter, spaced a few micrometers apart, in the implanted regions. The pits were attributed to the agglomeration of hydrogen, but whether the agglomerates were hydrogen-filled

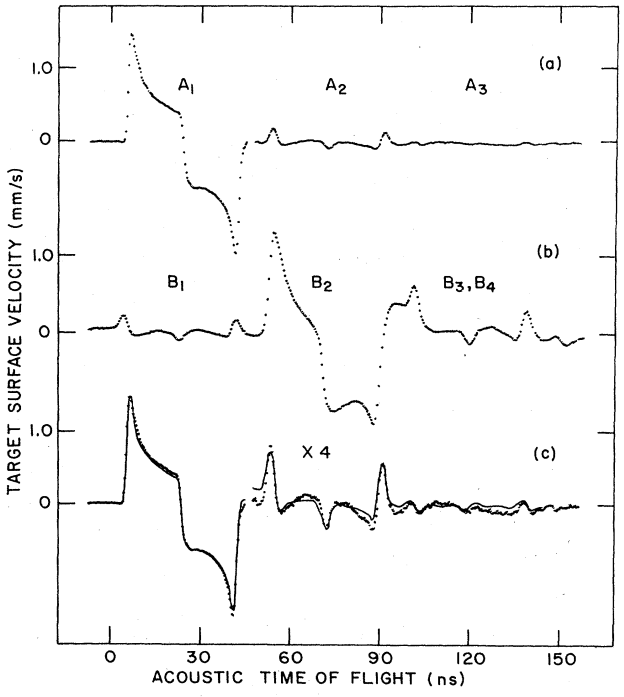

FIG. 5. (a) Acoustic signal generated by 3.74-MeV protons stopping in an aluminum target which had been implanted with 5×10^{18}/cm^2 of 4.39-MeV protons. (b) Reflected acoustic signal which arrives at the detector about 400 ns after the signal in (a). (c) Same signal as in (a), together with a calculated waveform. The vertical scale is expanded fourfold for the part following the primary signal.

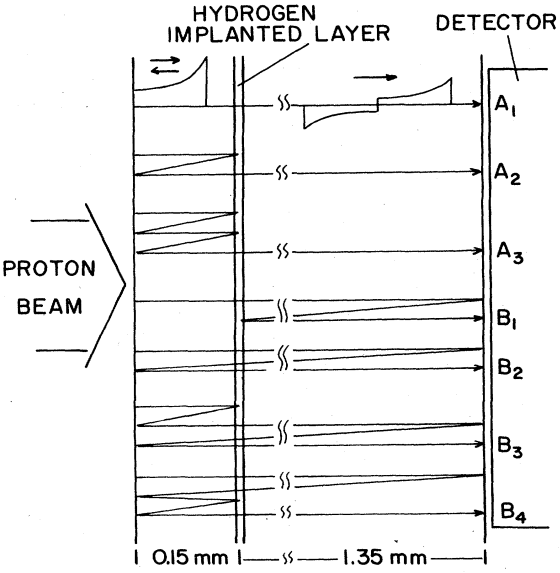

FIG. 6. Schematic illustration showing some of the possible acoustic paths in an implanted target. The labels are used to identify the corresponding signal components in Fig. 5.

voids could not be determined. Ells and Evans found that annealing of irradiated samples above 300 °C produced bubbles several micrometers in diameter.

The implanted region in the target of Fig. 5 contains hydrogen at a concentration of about 5×10^3 ppm (assuming a layer thickness of 6 μm due to range straggling of the implanting beam), which is much greater than the concentrations investigated by Ells and Evans. Milacek *et al.*[21] have investigated the blistering of aluminum samples implanted with hydrogen up to about 2×10^3 ppm, using up to 200-keV protons. Samples irradiated at proton energies of 100—200 keV blistered only after being annealed at 300 °C. For that case the blisters were 1 μm in diameter and were spaced about 1 μm apart. The observations of Milacek *et al.* and of Ells and Evans indicate that over a wide range of hydrogen concentrations in aluminum, the spacing of bubble nucleation centers is of the order of 1 μm.

How are the macroscopic elastic properties of a material altered by the presence of microbubbles? Mal and Knopoff[22] have derived a macroscopic wave equation for a uniform elastic matrix containing a random distribution of a small spherical inclusions. The two-component medium is assumed to be statistically homogeneous, and only wavelengths much larger than the diameter of any of the inclusions are considered. For a longitudinal plane wave traveling in the x direction, an average displacement of the form $\langle\xi(x)\rangle\exp(-i\omega t)$ resulting from multiple scattering satisfies

$$\langle E\rangle\nabla^2\langle\xi(x)\rangle+\omega^2\langle\rho\rangle\langle\xi(x)\rangle=0\ , \tag{11}$$

where $\langle E\rangle$ is the average effective modulus and $\langle\rho\rangle$ the average density of the two-component medium. For the case in which the inclusions are spherical voids, Mal and Knopoff have obtained

$$\langle E\rangle=E_0[1-f(\nu)\beta]\ , \tag{12}$$

where E_0 and ν are the plate modulus and Poisson's ratio for the medium without voids, and β is the average volume fraction occupied by voids. The factor $f(\nu)$ is given by

$$f(\nu)=\tfrac{1}{2}\left[\frac{1+\nu}{1-2\nu}\right]+\tfrac{10}{7}\left[\frac{1-2\nu}{1-5\nu/7}\right]\ . \tag{13}$$

In aluminum $\nu=0.346$ (Ref. 23), for which value $f=2.77$.

Gas-filled bubbles can be treated as voids if the pressure inside a bubble is not too great. The equilibrium pressure inside a bubble of radius r is $p=2\gamma/r$, where γ is the surface tension, Greenwood *et al.*[24] have estimated that nearby dislocations can permit a bubble to expand through plastic deformation when p satisfies

$$p-2\gamma/r>\mu b/r\ , \tag{14}$$

where b is the Burger's vector. In aluminum $b=3.4\times10^{-8}$ cm, $\mu=2.5\times10^{11}$ dyne/cm^2 (Ref. 23), and a value of $\gamma=860$ ergs/cm^2 has been measured in molten aluminum.[25] For a bubble in aluminum of radius 0.1 μm, this mechanism for expansion prevents the pressure from greatly exceeding 10^3 atm which is about 10^3 times smaller than the bulk modulus of aluminum. Consequently, in our analysis we treat hydrogen bubbles as empty voids.

An implanted target can be described macroscopically as an elastic medium whose density and elastic moduli vary with depth. For longitudinal waves propagating normal to the target surface, a simple analysis leads to the following wave equation for the displacement $\xi(x,t)$:

$$\rho(x)\frac{\partial^2\xi}{\partial t^2}-E(x)\frac{\partial^2\xi}{\partial x^2}-\frac{\partial E}{\partial x}\frac{\partial\xi}{\partial x}=0\ . \tag{15}$$

Suppose that the distribution of bubbles in a target can be described macroscopically by an average volume fraction $\beta(x)$. If changes in β are small over a distance of the order of the bubble spacing, then the modulus $E(x)$ can be obtained through Eq. (12). The target density is $\rho(x)=\rho_0[1-\beta(x)]$, where ρ_0 is the density of the matrix material.

Hydrogen implanted targets were modeled by assuming $\beta(x)$ to be a Gaussian function whose width and amplitude could be inferred from the acoustic data. The signal in Fig. 5(a) is shown again in 5(c) together with a model waveform which was obtained in a similar manner as for those of Fig. 4, except that the propagation of the initial pressure distribution was determined by solving Eq. (15) numerically. A layer thickness of 9 μm full width at half maximum (FWHM) was chosen to fit the width of the peaks in the observed reflection from the implanted layer. The amplitude of the reflected signal was then fit by choosing a fractional bubble volume of 11% corresponding to a 21% reduction in acoustic impedance, at the center of the layer. Since the range straggling of the implanting beam is about 6 μm (FWHM), our analysis indicates that hydrogen has diffused and formed bubbles outside the region of implantation. It should be noted here that since the inferred layer width is about 10 times the bubble spacing (~1 μm), our use of Eqs. (11) and (12), which are based on multiple scattering, is physically reasonable. Measurements were made on several other implanted aluminum targets with doses from 2×10^{18} to 11×10^{18} protons/cm^2. In those targets the total bubble volumes inferred from acoustic measurements were found to be roughly proportional to the implantation dose.

After measurements at room temperature were made on the target of Fig. 5, the acoustic signal was monitored while the target was heated in place. Figure 7 shows the relative amplitude of the reflection from the bubble layer as the target was heated from room temperature to 126 °C over a period of two hours. The signal showed little change up to about 90 °C, but above 90 °C it appears that the volume of bubbles in the implanted layer increased much more rapidly. Subsequent heating of the target to 139 °C caused the aluminum matrix to fail and a blister to form in the implanted layer (see Ref. 11).

Observations of bubble growth can provide information about the diffusion of hydrogen in aluminum. The simplest model of diffusion assumes that an atom will move from its site whenever its kinetic energy exceeds a barrier potential U (called the activation energy). The diffusivity then has the form[26]

$$D=D_0\exp(-U/kT)\ , \tag{16}$$

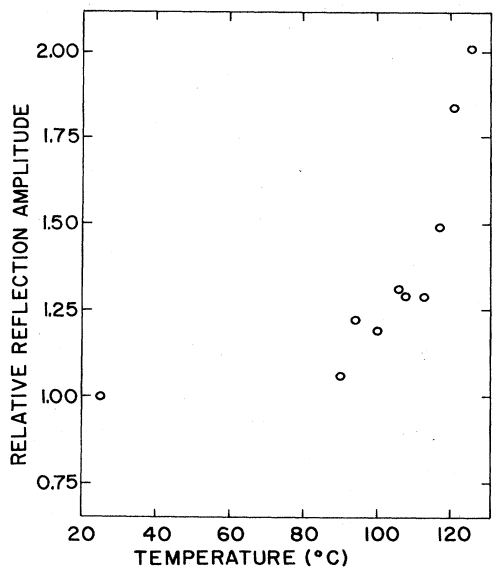

FIG. 7. Relative amplitudes for the acoustic signal reflected by the implanted layer in the target of Fig. 5, plotted vs temperature. The target was heated from room temperature to 126 °C over a period of about 2 h.

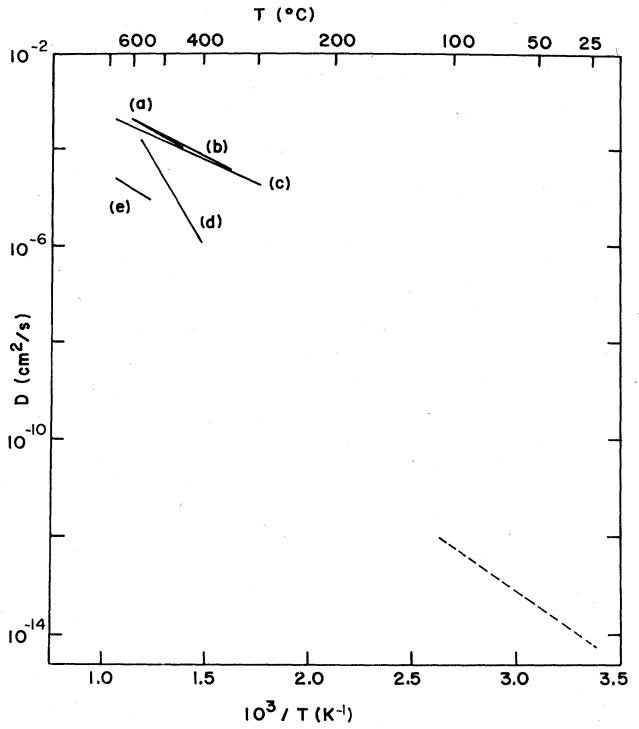

FIG. 8. Diffusivity of hydrogen in aluminum estimated from acoustic observation (dashed line), together with several measurements of diffusivity reported in the literature: (a) Eichenauer and Pebler (Ref. 28), (b) Eichenauer *et al.* (Ref. 29), (c) Ichimura *et al.* (Ref. 30), (d) Ransley and Talbot (Ref. 31), and (e) Matsuo and Hirata (Ref. 32).

where T is the absolute temperature. The average time required for an atom to diffuse beyond a distance R from its starting point is about $R^2/4D$ (Ref. 27). Assuming that bubble nucleation centers are spaced about 1 μm apart, we can estimate that significant bubble growth occurs in hydrogen-implanted aluminum in a time t_0 given by $(4Dt_0)^{1/2}=1$ μm. Acoustic reflection from bubble layers were not observed to change over periods of up to 10 h. Measurements made several days after implantation, however, indicated increases in bubble volumes of up to 50%. Thus at room temperature (25 °C) $t_0 \cong 100$ h. From the measurements of Fig. 7 it appears that $t_0 \cong 1$ h at 100 °C. Using these estimates in Eq. (16) gives $D_0=6\times10^3$ cm^2/s and $U=0.59$ eV. The resulting diffusivity is plotted in Fig. 8 (dashed line). Also shown in Fig. 8 are several measurements of hydrogen diffusivity in aluminum reported in the literature. Those measurements were all made at elevated temperatures (>300 °C), where the diffusivity is much larger than at room temperature. In measurements (a), (b), and (c) samples from molten aluminum cooled in vacuum were used, and for those cases the results are in reasonable agreement. Lower values of diffusivity were obtained in measurements (d) and (e), for which the aluminum samples were not vacuum cast. The discrepancies are attributed by Ichimura *et al.*[30] to voids in the aluminum, caused by gases trapped during fabrication. In our experiments we used type 1100 aluminum ($>99\%$ pure), which may contain various impurities. Also, the radiation damage due to the implanting beam is greatest in the region where we were observing hydrogen bubble growth. Conceding these limitations, we have observed hydrogen diffusion in aluminum in a regime where the diffusivity is 8—10 orders of magnitude smaller than in previous measurements.

VI. CONCLUSIONS

We have presented time-resolved measurements of acoustic signals generated by a pulsed proton beam stopping in aluminum. The shapes of acoustic pulses observed traveling in the beam direction are in good agreement with the thermoelastic model of sound generation. From the signal rise time (<2 ns), it can be concluded that the conversion into heat of the energy loss of a slowing proton is localized within a radius of several micrometers. The amplitudes of the signals we observe are in agreement with the thermoelastic model within the uncertainty ($\sim10\%$) of the absolute measurement.

From observations of the scattering of acoustic pulses in hydrogen-implanted aluminum, we have determined the fractional volume occupied by hydrogen microbubbles and the thickness of the bubble layer. From bubble growths inferred from acoustic measurements we have estimated the diffusivity of hydrogen in aluminum at much lower temperatures (~25—100 °C) than the temperatures used in other studies.

The sensitivity of our detector is about 20 μV/(mm/s). Thus, one of the small velocity peaks in Fig. 5 (~0.2 mm/s for 5 ns) generates in the detector an electrical energy of about 10^{-2} eV. Of course, such a small signal can be observed only by averaging the detector output over many beam pulses.

The fraction of beam-pulse energy converted to sound energy in a target is Kq, where q is the density of energy deposition, and K depends on the thermal and mechanical properties of the target material. For the signals shown in Sec. IV, this energy fraction is about 10^{-7}. The fraction of incident sound energy that is converted in the detector to electrical energy is

$$r=4\epsilon\frac{\mathscr{E}^2}{Z_l}\frac{RC}{L}\ , \tag{17}$$

where Z_l is the acoustic impedance of the target material, ϵ is the permittivity and $\mathscr{E}$ is the applied electric field in the dielectric, and $\mathscr{E}L$ is the detector bias. Thus, if the time constant RC is limited by the bandwidth requirement, then the detector sensitivity is determined by the properties of the dielectric (permittivity, thickness, and breakdown field). For the detector we have constructed $r=5\times10^{-7}$ for an aluminum target. Thus, assuming that most of the acoustic flux is incident on the detector, the fraction of beam energy absorbed from acoustic radiation by the detector is about 5×10^{-14}.

ACKNOWLEDGMENTS

This work was supported by the National Science Foundation under Grants Nos. PHY-81-00214 and PHY-83-06683.

*Present address: Lawrence Livermore National Laboratory, Livermore, CA 94550.

[1]L. Sulak, T. Armstrong, H. Baranger, M. Bregman, M. Levi, D. Mael, J. Strait, T. Bowen, A. E. Pifer, P. A. Polakos, H. Bradner, A. Parvulescu, W. V. Jones, and J. Learned, Nucl. Instrum. Methods **161**, 203 (1979).

[2]P. I. Golubnichii, G. S. Kalyuzhnyi, S. D. Korchikov, V. V. Petrenko, and V. N. Yakovlev, Pis'ma Zh. Tekh. Fiz. **7**, 272 (1981) [Sov. Tech. Phys. Lett. **7**, 117 (1981)].

[3]B. L. Beron, S. P. Baugh, W. O. Hamilton, R. Hofstadter, and T. W. Martin, IEEE Trans. Nucl. Sci. **NS-17**, 65 (1970).

[4]V. D. Volovik and V. T. Lazurik-Él'tsufin, Fiz. Tverd. Tela (Leningrad) **15**, 2305 (1973) [Sov. Phys.—Solid State **15**, 1538 (1974)].

[5]F. C. Perry, Appl. Phys. Lett. **17**, 408 (1970).

[6]A. De Rujula, S. L. Glashow, R. R. Wilson, and G. Charpak, Phys. Rep. **99**, 343 (1983). Quote from p. 363.

[7]W. B. Gauster and M. A. Breazeale, Rev. Sci. Instrum. **37**, 1544 (1966).

[8]J. H. Cantrell and M. A. Breazeale, J. Acoust. Soc. Am. **61**, 403 (1977).

[9]A. C. Tam and H. Coufal, Appl. Phys. Lett. **42**, 33 (1983).

[10]G. E. Sieger, Ph.D. thesis, University of Oregon, pp. 5—19, 1983 (unpublished).

[11]G. E. Sieger and H. W. Lefevre, Appl. Phys. Lett. **44**, 28 (1984).

[12]D. C. Forster, in *The Encyclopedia of Electronics,* edited by Susskind (Reinhold, New York, 1962), p. 553.

[13]W. C. Elmore and M. A. Heald, *Physics of Waves* (McGraw-Hill, New York, 1969), p. 229.

[14]G. A. Askariyan, B. A. Dolgoshein, A. N. Kalinovsky, and N. V. Makhov, Nucl. Instrum. Methods **164**, 267 (1979).

[15]J. M. Liu, R. Yen, H. Kurz, and N. Bloembergen, Appl. Phys. Lett. **39**, 755 (1981).

[16]J. Opsal and A. Rosencwaig, J. Appl. Phys. **53**, 4240 (1982).

[17]A. Rosencwaig, Science **218**, 223 (1982).

[18]Recorded voltage signals were corrected for the distortion due capacitive coupling of the detector output, and from those results velocity signals were inferred through Eq. (2).

[19]H. H. Andersen and J. F. Ziegler, *Hydrogen Stopping Powers and Ranges in all Elements* (Pergamon, New York, 1977), Vol. 3.

[20]C. E. Ells and W. Evans, Trans. Metall. Soc. AIME **227**, 438 (1963).

[21]L. H. Milacek, R. D. Daniels, and J. A. Cooley, J. Appl. Phys. **39**, 2803 (1968).

[22]A. K. Mal and L. Knopoff, J. Inst. Math. Appl. **3**, 376 (1967).

[23]G. Simmons and H. Wang, *Single Crystal Elastic Constants and Calculated Aggregate Properties: A Handbook,* 2nd ed. (MIT, Cambridge, Mass., 1971), pp. 155—160.

[24]G. W. Greenwood, A. J. E. Foreman, and D. E. Rimmer, J. Nucl. Mater. **1**, 305 (1959).

[25]A. M. Korol'kov, Izvest. Akad. Nauk S.S.S.R., Otdel. Tekh. Nauk **2**, 35 (1956) [Chem. Abstr. **50**, 10471 (1956)].

[26]C. Kittel, *Solid State Physics,* 5th ed. (Wiley, New York, 1976), p. 543.

[27]W. Feller, *An Introduction to Probability Theory and Its Applications,* 3rd ed. (Wiley, New York, 1968), Vol. I, Chap. XIV.

[28]W. Eichenauer and A. Pebler, Z. Metallkd. **48**, 373 (1957) [Chem. Abstr. **52**, 2488 (1958)].

[29]W. Eichenauer, K. Hattenbach, and A. Pebler, Z. Metallkd. **52**, 682 (1961) [Chem. Abstr. **56**, 7023 (1962)].

[30]M. Ichimura, M. Imabayashi, and M. Hayakawa, J. Jpn. Inst. Met. **43**, 876 (1979).

[31]C. E. Ransley and D. E. J. Talbot, Z. Metallkd. **46**, 328 (1955) [Chem. Abstr. **49**, 10696 (1955)].

[32]S. Matsuo and T. Hirata, J. Jpn. Inst. Met. **31**, 590 (1967) [Chem. Abstr. **67**, 6391 (1967)].